

Coupled resonators based on high permittivity dielectrics for microwave sensors

Shahnam Gorgi Zadeh,^{1,*} Alberto Gherri,^{2,†} Sergio Pagano,³ Simone Tocci,⁴ Claudio Gatti,⁴ and Antonio Cassinese⁵

¹*European Organization for Nuclear Research (CERN), Meyrin 1217, Switzerland*

²*Istituto Nanoscienze - CNR, Centro S3, via G. Campi 213/A, 41125, Modena, Italy*

³*Physics Department and INFN GC Salerno, University of Salerno,
via Giovanni Paolo II 132, Fisciano (SA), Italy*

⁴*INFN, National Institute for Nuclear Physics, I-00044, Frascati, Italy*

⁵*Physics Department and INFN -Napoli, Università Napoli Federico II, P.le Tecchio 80, 80125 Naples, Italy*

The use of coupled cavities with high quality factor is of undoubted interest for several applications including those concerning quantum sensing and metrology. Here we report on a coupled cavity configuration in which a high Q -factor elliptical TESLA-shaped superconducting cavity is coupled with a high permittivity (ϵ_r) dielectric resonator. We carried out first tests using a SrTiO₃ (STO) resonator at 0.1 GHz, whose permittivity has been observed to reach values higher than 30000 at 0.16 K. The sensitivities of such configurations are discussed both in strong coupling and weak coupling regime. In particular we show that the notch of the coupled system has, as a function of the permittivity, a frequency sensitivity of 2.8 MHz for $\epsilon_r \approx 230$. These results highlight the potential of the coupled resonator systems as microwave sensors and are useful for the engineering of high permittivity resonators for applications at cryogenic temperatures.

I. INTRODUCTION

Resonant cavities, with their ability to sustain high electromagnetic fields, have emerged as powerful tools for ultra-sensitive measurements. These structures, also known as resonators, operate by confining electromagnetic waves within a bounded region, allowing for resonance at specific frequencies. The high-quality factors (Q -factors) associated with resonant cavities enable precise frequency measurements and enhanced sensitivity, making them indispensable in various scientific and engineering applications.

The use of resonant cavities for sensitive measurements has a rich history, particularly in the fields of fundamental physics, metrology, and quantum mechanics. For instance, early work by Pound and Rebka (1959) demonstrated the potential of resonant cavities to detect extremely small frequency shifts, paving the way for their use in precision measurement [1]. In the field of particle physics, high- Q microwave cavities have been instrumental in the search for axions, hypothetical particles proposed as dark matter candidates [2, 3]. Similarly, resonant cavities are used in experiments testing the fundamental constants of nature, providing critical tests of physical theories beyond the Standard Model [4–6]. In quantum information science, superconducting microwave cavities are employed to couple qubits and facilitate quantum state readout with high fidelity [7, 8]. Furthermore, hybrid quantum systems combining resonant cavities with other quantum technologies, such as optomechanical or spin systems such as nitrogen-vacancy centers in diamond, have shown promise for enhanced sensitivity in detecting weak forces and fields. These hy-

brid systems leverage the strong coupling between cavity modes and quantum states to achieve unprecedented measurement sensitivity [9]. The inherent sensitivity of resonant cavities also extends to applications in precision spectroscopy and time-keeping [10–12].

Unlike the power detection scheme, the fundamental limit in frequency measurements comes from the best achievable frequency stability of the measurement parts and thus it is not directly related to the Nyquist noise and the ambient temperature, although cryogenic cooling may significantly improve the detection limit due to higher quality factors. It is generally accepted that one can detect frequency variations on the order of 10^{-6} relative to the system bandwidth. With systems such as superconducting cavities and sapphire, it is possible to achieve bandwidths of the order of 1 Hz at microwave frequencies giving unprecedented sensitivity of the frequency measurement approach.

The coupling of two, or more, resonators introduce further versatility that can be exploited for several of the above-mentioned applications of high- Q resonators [13–17]. In particular, superconducting TESLA cavities, which were developed in the context of particle accelerators with Q -factors larger than 10^9 [18], were coupled in different means showing that the photon lifetime of the local field can exceed that of the bare cavities [19]. Additionally, coupled sapphire resonators were proposed for high sensitivity axion detection systems based on the increased Q -factor and tunability due to the supermode effect [20]. Systems composed of coupled dielectric resonators were also proposed for the bolometric detection of particles and X-ray photons [21–23]. Here, a first sapphire resonator that acts as a stable reference frequency is coupled to a second resonator having a strongly temperature-dependent permittivity (e.g. CaTiO₃ or SrTiO₃). The absorption of energy causes a change in the absorber's permittivity, in turn

* shahnam.zadeh@uni-rostock.de

† alberto.gherri@nano.cnr.it

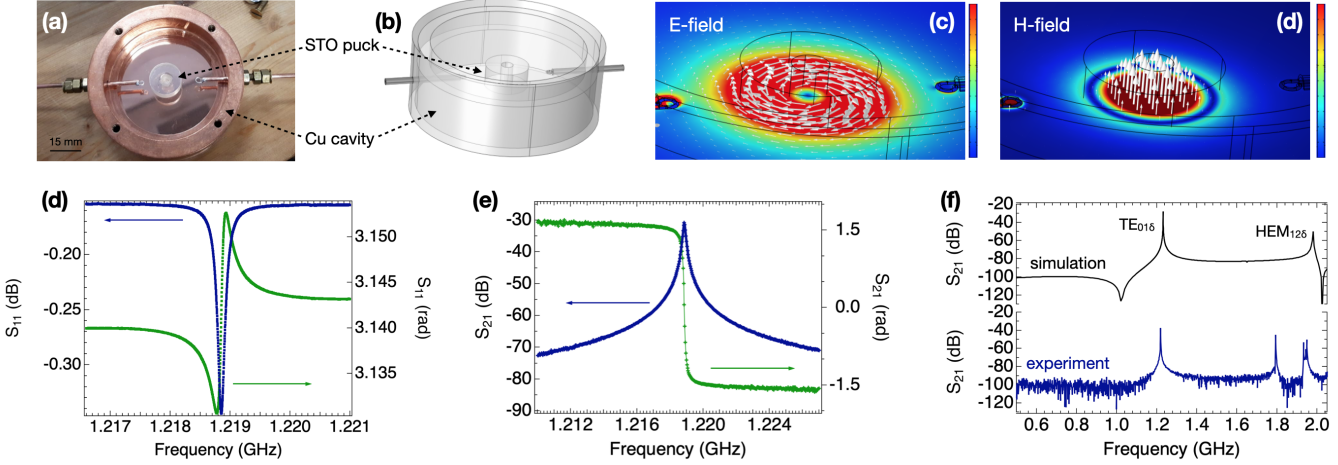


FIG. 1. Characterization of the STO resonator at room temperature. (a) Photograph showing the STO puck and Cu cavity used in the experiments. (b) Sketch of the model used for simulations (COMSOL Multiphysics). The top cap is not shown. (c,d) Simulated distribution of the root-mean-square electric and magnetic field for the TE_{01δ} mode ($\epsilon_r = 318$). (d,e) Plots of reflection (S_{11}) and transmission spectra (S_{21}) measured at room temperature (incident power 0 dBm). The amplitude is shown in blue, the phase in green. (f) Comparison between experimental and simulated S_{21} spectra.

producing a measurable change in the resonant frequency of the coupled system.

Dielectric resonators have attracted long time interest for several applications in sensing, metrology and detectors due to their well defined resonant modes and high Q -factors. High permittivity materials such as SrTiO₃, KTaO₃, LaAlO₃ and TiO₂ have been used in different situations, including room-temperature masers [24], dark matter searches [25] quantum sensing [26] and spin manipulation [27]. In particular, strontium titanate (SrTiO₃) has been the subject of intense study because of its peculiar physics [28], characterized in particular by quantum paraelectricity [29–31] and superconductivity [32] at low temperature, and emergent conductivity or magnetism at the interface with other oxides, i.e. in LaAlO₃/SrTiO₃ heterostructures [28]. The properties of SrTiO₃ at microwave frequencies were also investigated [33–35], recently reporting also the anomalous behavior of complex permittivity below 1 K [36, 37].

Here we report a study of the coupling between an elliptical TESLA-shaped cavity at 1.3 GHz and a strontium titanate (hereafter STO) dielectric resonator. We first report microwave measurements on a STO puck, which were carried out to characterize the dielectric resonator and test the evolution of permittivity and losses at temperatures down to 150 mK. We then exploit finite-element electromagnetic simulations to study the coupling between elliptical TESLA-shaped cavity and dielectric resonator, discussing the evolution of frequency and Q -factor of the coupled modes as a function of geometric and material parameters, such as the position of the STO puck within the cavity and the frequency of the STO resonator. We finally report room temperature test measurements carried out with a metallic elliptical cavity and the STO resonator, which are compared to the outcome

of finite-element simulations. Overall, these results define key parameters to control the coupling between high- Q cavities and high permittivity dielectric resonators, opening a path for the exploitation of these systems as microwave sensors in particle detection, quantum sensing and metrology experiments.

II. CHARACTERIZATION OF THE STO RESONATOR

The dielectric resonator was realized with a STO crystal produced by SurfaceNet GmbH that was shaped into a cylinder having radius $a=8.17$ mm and height $d=7.26$ mm, with a central hole of radius 2 mm. For the characterization of the dielectric resonator we used a hollow copper cavity (inner radius 60 mm, height 22 mm), whose lowest mode at 3.8 GHz stands well above the fundamental mode of the dielectric resonator in order to avoid cross couplings between their modes. The STO puck was installed on top of two quartz pillars and coupled to the coaxial lines by loop antennae positioned at a distance of 10–20 mm from the outer surface of the cylinder (Fig. 1(a)). The whole set-up was measured at room temperature, in liquid nitrogen and in the 0.15–10 K temperature range by means of a dilution fridge.

Room temperature measurements. Reflection and transmission spectra acquired at room temperature show the fundamental mode of the STO resonator at frequency $f_0 = 1.22$ GHz (Fig. 1(d,e)). Considering the geometric factors of the resonator and the STO permittivity $\epsilon_r \approx 318$, we obtain that f_0 corresponds well with the frequency of the TE_{01δ} mode derived by semi-analytical formulae [38, 39]. The loaded quality factor extracted from the transmission spectrum (Fig. 1(e)) is $Q_L = 8000$.

Since the coupling between feedlines and resonator is small, the internal quality factor in good approximation is $Q_0 \approx Q_L \approx 1/\tan \delta$. The loss tangent of STO thus results $\tan \delta = 1.2 \times 10^4$. Finite-element electromagnetic simulations confirm the distribution expected for the $TE_{01\delta}$ mode (Fig. 1(c,d)), whose frequency results about 1.2 GHz in close agreement with the experimental data (Fig. 1(f)).

Low temperature behavior. The microwave dielectric properties of STO have been reported between 4 and 300 K by investigating the temperature evolution of the modes of cylindrical STO crystal specimens [33–35]. In this temperature range the maximum Q -factor value was 20000 reached around 100 K just above the structural temperature transition of STO. The nonlinear change in the permittivity of STO encompasses two orders of magnitude to reach $\epsilon_r \approx 3 \times 10^4$ and $\tan \delta \approx 1 \times 10^{-3}$ at 5 K [33]. The ferroelectric phase transition temperature takes place around 51 K, while the quantum paraelectric phase stabilizes below 5 K [34].

We tested the STO resonator at temperatures below 1 K (Fig. 2). The STO resonator was installed in a dilution fridge and slowly cooled down to 150 mK in about 6 hours. The temperature was measured by using a thermometer installed into the copper cavity. At the lowest temperature, the $TE_{01\delta}$ mode frequency resulted $f_0 = 116.9$ MHz with $Q \approx 1 \times 10^4$; these values suggest $\epsilon_r \approx 3 \times 10^4$ and $\tan \delta \approx 1 \times 10^{-4}$. As a function of the decreasing temperature, the frequency of the $TE_{01\delta}$ mode decreases until 0.4 K, while for lower temperatures we observe a slight upturn.

III. COUPLED STO AND ELLIPTICAL CAVITY

This section examines the coupling of the STO puck with a resonating cavity to form a coupled resonator system. To facilitate this investigation, we selected an elliptical TESLA-shaped cavity [18] operating at 1.3 GHz. This frequency was selected because it closely matches the operational frequency of the available STO puck sample at room temperature and because similar elliptical cavity prototypes were available for measurement at the European Organization for Nuclear Research (CERN). However, it is important to emphasize that the choice of cavity and frequency is not limited to the elliptical cavity at 1.3 GHz; other cavity types and frequencies may be used based on specific project requirements. The primary aim of this study is to assess the feasibility of coupling between the STO puck and a superconducting RF cavity.

Electromagnetic simulations. The TESLA-shaped elliptical cavity and its fundamental mode (FM), which is a transverse magnetic (TM) mode, are illustrated in Fig. 3. The cavity's equator radius was adjusted to achieve a frequency of 1.3 GHz. For a copper cavity, the quality factor of this mode is 2.89×10^4 . At room temperature, with $\epsilon_r = 318$, the first mode of the STO puck has a frequency of 1.10 GHz and a quality factor of 1.01×10^4 . The field

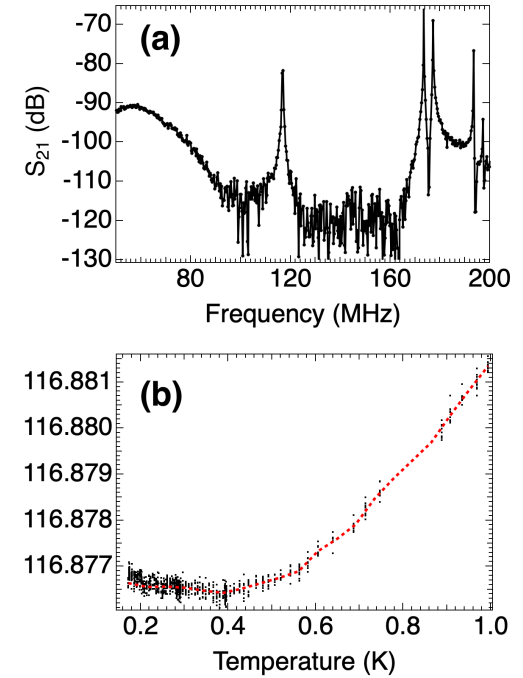


FIG. 2. Characterization of the STO resonator at temperature below 1 K. (a) Transmission spectrum acquired at 170 mK. (b) Temperature dependence of the fundamental mode frequency. The red dashed line shows the interpolation of the experimental points.

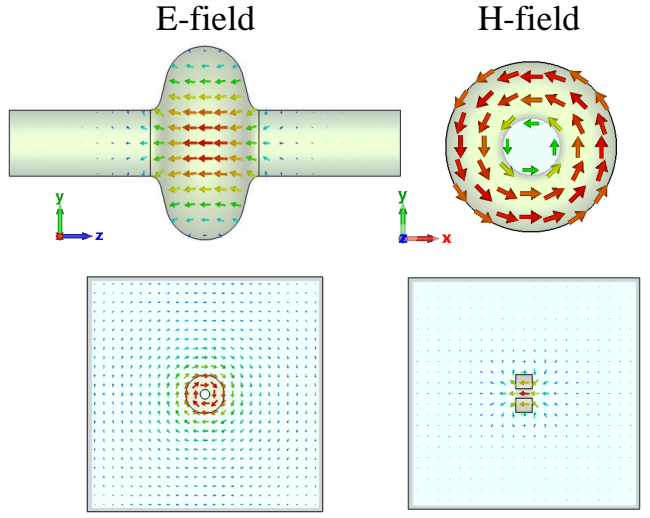
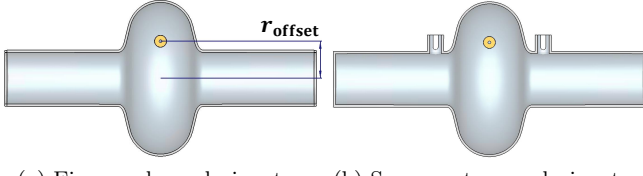


FIG. 3. The field distribution of the TM_{010} mode in a TESLA-shaped 1.3 GHz accelerating cavity (top) and the first mode of the STO puck (bottom).

plot of this mode is also shown in Fig. 3. To investigate the coupling between the two modes, the STO puck is placed inside the elliptical cavity. Two essential parameters for effective coupling are the orientation of the STO puck within the elliptical cavity and its radial offset from



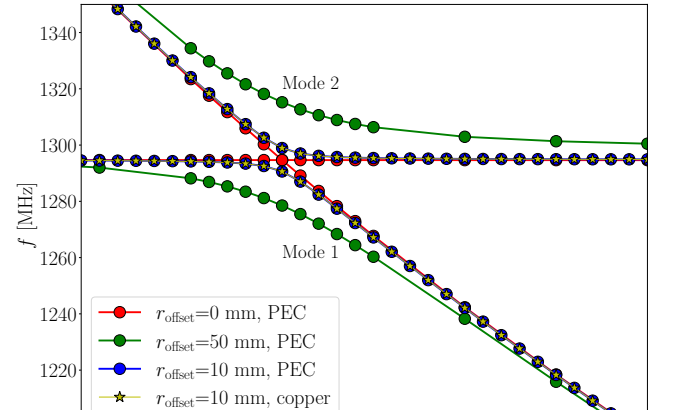
(a) Eigenmode analysis setup (b) S-parameters analysis setup

FIG. 4. Simulation setups of the coupled elliptical cavity and STO puck. The radial offset of the STO puck (r_{offset}) influences the coupling strength between the two modes.

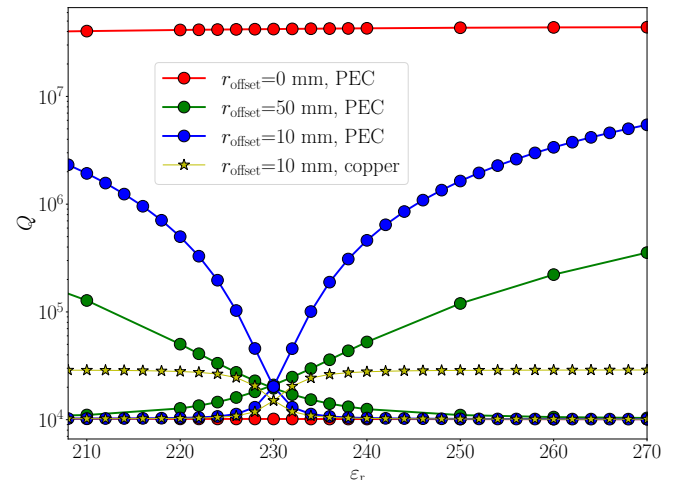
the center. The puck's position in the elliptical cavity for effective coupling is shown in Fig. 4. Coupling is examined using both eigenmode analysis and frequency domain analysis, with two identical antennas, each having $Q_{\text{ext}} = 8.6 \times 10^7$. In the eigenmode analysis, no antennas are considered, and the only losses accounted for are the dielectric losses of STO and surface losses on the elliptical cavity if non-perfect electric conductor (PEC) materials are used.

The results of the eigenmode analysis are presented in Fig. 5. The investigation examines how varying ϵ_r of the STO, which can be a function of temperature, affects the resonant frequency and Q -factor of the first two modes in the coupled system. The STO-dominant mode is characterized by having most of its energy localized in the STO, while the elliptical cavity-dominant mode retains most of its energy within the elliptical cavity, similar to the uncoupled system. Below $\epsilon_r = 230$, Mode 2 is the STO-dominant mode and Mode 1 is the elliptical cavity-dominant mode. Above $\epsilon_r = 230$, the order of the modes is reversed. When $r_{\text{offset}} = 0$ mm, the two modes do not interact as ϵ_r changes. In this scenario, the elliptical cavity's frequency and Q -factor remain nearly constant at 1.3 GHz and $Q_{\text{ext}} = 4.2 \times 10^7$, respectively, for a PEC cavity. In this PEC situation, the Q -factor value is influenced by the losses in the dielectric region occupied by the STO puck. Conversely, the frequency of the STO-dominant mode decreases with increasing ϵ_r , while its Q -factor remains nearly constant at $Q_{\text{ext}} = 1.0 \times 10^4$. In this scenario, the frequencies of the elliptical cavity-dominant mode at 1.3 GHz and the STO-dominant mode are unaffected by each other and intersect at $\epsilon_r = 230$, with no interaction between the modes as ϵ_r changes. The permittivity value of 230 corresponds to a temperature above room temperature, even though the system is ideally intended for operation at lower temperatures where the STO's resonance frequency exhibits the greatest sensitivity to temperature variations (around 25 K). However, due to the fixed dimensions of the STO puck and the elliptical cavity's frequency, we adjust the STO permittivity to shift its resonance frequency near 1.3 GHz to investigate the mode coupling between the two resonators.

When the STO puck is radially offset, mode splitting occurs at $\epsilon_r = 230$, and the interaction between the two



(a) Frequency of eigenmodes



(b) Quality factor of eigenmodes

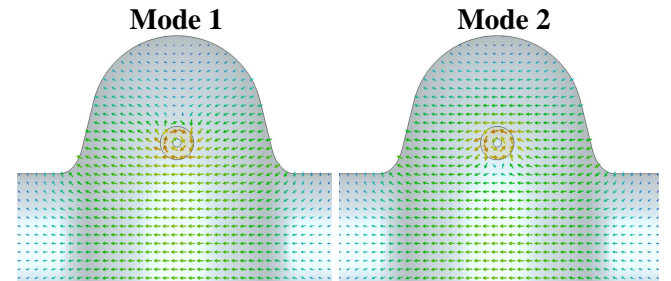
(c) E-field plots of the two modes at $\epsilon_r = 230$ and $r_{\text{offset}} = 50$ mm

FIG. 5. Parameter sweep of the dielectric constant (ϵ_r) of STO and its effect on the frequency and quality factor of the first two modes of the coupled elliptical cavity and STO puck at different radial offset (r_{offset}) values. Mode 1 is the mode with the lower frequency.

modes intensifies as the radial offset increases from zero. The level repulsion, defined as the distance between the two dispersion curves, grows with larger radial offsets, indicating stronger coupling between the two modes. This coupling causes the Q -factor of the STO-dominant mode

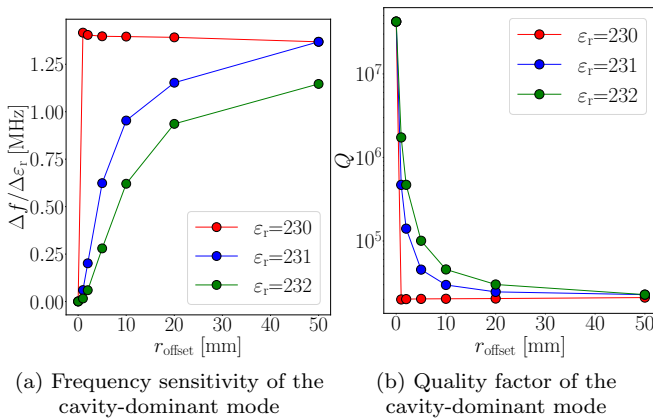


FIG. 6. Dependency of the frequency sensitivity and quality factor of the elliptical cavity-dominant mode with respect to r_{offset} .

(low- Q mode) to increase, while the Q -factor of the elliptical cavity-dominant mode (high- Q mode) decreases, and both converge at $\epsilon_r = 230$. For a PEC elliptical cavity and an STO puck with $r_{\text{offset}} = 50$ mm and $\epsilon_r = 230$, the two modes exhibit equal quality factors of approximately $Q = 2 \times 10^4$. One mode has a frequency of 1279 MHz, while the other is at 1315 MHz. The field plots for these two modes are presented in Fig. 5(c). In addition to changes in ϵ_r , the eigenmode frequency sensitivities and their quality factors also depend on the radial offset. As shown in the Fig. 6, at $\epsilon_r = 230$, where the coupling is at its maximum, even a slight radial offset of the puck results in a sharp reduction in the quality factor of the elliptical cavity-dominant mode. This is followed by an increase in the mode's frequency sensitivity to changes in ϵ_r .

In practice, eigenmode information is obtained through S-parameter measurements. Figure 7 illustrates the S-parameters for an excitation scheme using two antennas (as shown in Fig. 4), with a puck offset of 50 mm. Two key parameters in the measurement are the frequency sensitivity of the modes to variations in ϵ_r and the Q -factor of the modes. The quality factor can be calculated using a 3 dB method and is also related to phase variations in the $S_{1,2}$ curve; larger phase changes (i.e., a steeper phase derivative) correspond to a higher Q -factor. Using the phase derivative offers the benefit of not only analyzing the peaks but also assessing the sensitivity of the notch. This notch, located between two resonance peaks in the S-parameters, corresponds to a point of minimal signal transmission.

Figure 7(c) illustrates the phase derivatives of the PEC cavity at various values of ϵ_r . The distribution or pattern of the phase derivative near resonance frequencies exhibits a Lorentzian shape. For modes near 1.3 GHz (corresponding to the elliptical cavity's dominant mode), the phase derivative amplitude shows high values, indicating a large Q -factor. For the notch mode, the phase

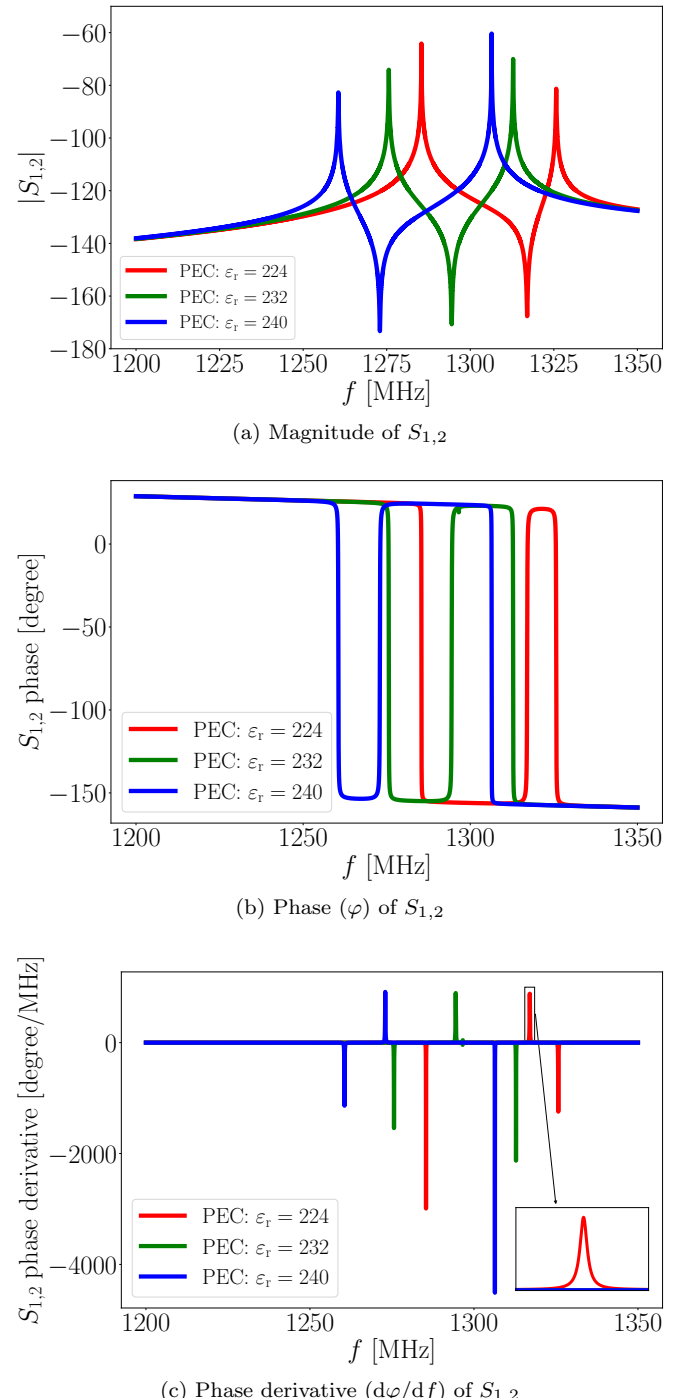
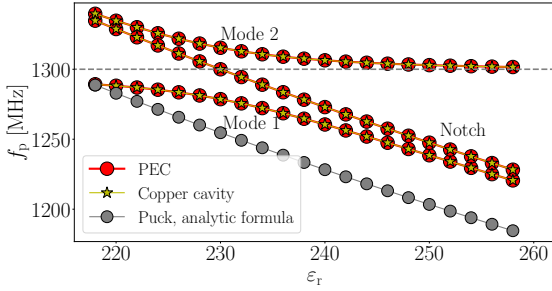
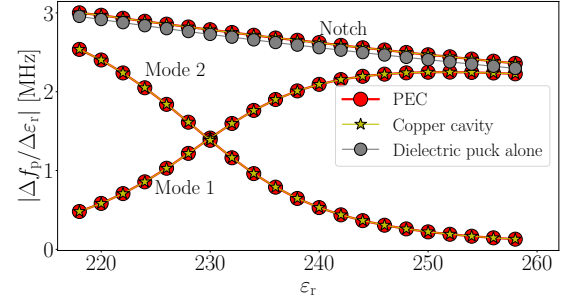


FIG. 7. S-parameters of the excitation scheme shown in Fig. 4 at different ϵ_r and $r_{\text{offset}} = 50$ mm for a PEC cavity. Varying ϵ_r shifts the resonance frequencies of the two peaks and the notch. The phase derivative (c) is linked to the quality factor, with higher amplitude for the mode with the larger Q -factor, and shows minimal change at the notch as ϵ_r varies.

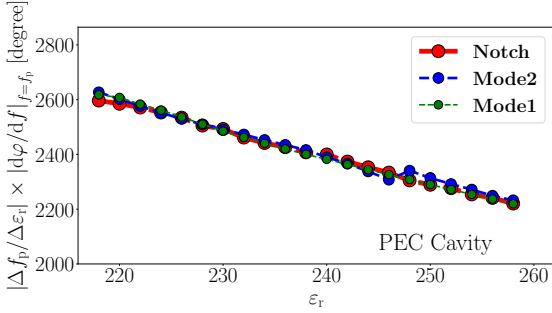
derivative peak remains nearly constant across different values of ϵ_r . For a normal conducting cavity, such as copper, the S-parameters are similar; however, the phase derivative amplitudes at the peaks are smaller, indicating



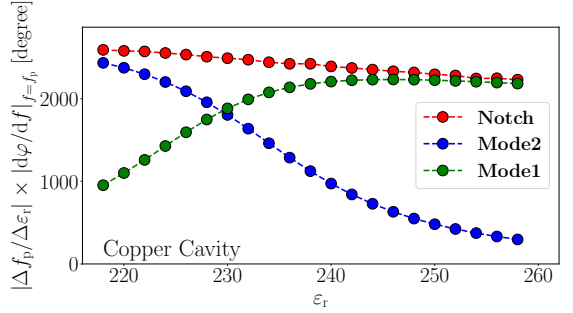
(a) Frequencies of the first and second peaks, as well as the notch, of the $|S_{1,2}|$ curves shown in Fig. 7(a)



(b) Derivative of the curves shown in (a)



(c) PEC cavity: curves in (b) times phase derivative at $f = f_p$ taken from Fig. 7(c)



(d) Copper cavity: curves in (b) times phase derivative at $f = f_p$ taken from Fig. 7(c)

FIG. 8. Analysis of the S-parameters shown in Fig. 7. Mode 1 and Mode 2 correspond to the frequencies of the first and second peaks of the $|S_{1,2}|$ curves, respectively, and the notch corresponds to the frequency of the dip between these two peaks. The frequency of the puck alone and its derivative calculated by the semi-analytic formula is also shown in (a) and (b). The product of frequency sensitivity and the maximum phase derivative at resonances and the notch is shown in (c) and (d) for the PEC and copper cavities, respectively. This term is almost equal at the notch for both the PEC and copper cavities. However, for modes 1 and 2, it is smaller in the copper cavity compared to the PEC cavity near ϵ_r of 230, where the coupling is at its maximum.

a lower Q -factor.

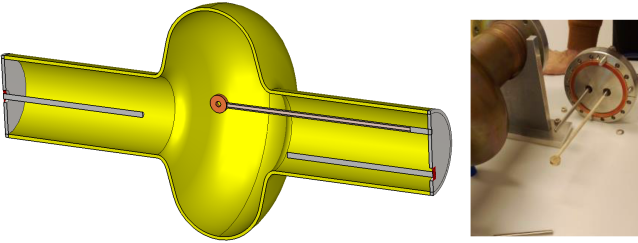
Figure 8 presents the frequencies of the two peaks in the $S_{1,2}$ curve, along with the notch between them. The resonance behavior as a function of ϵ_r resembles eigenmode analysis, with level repulsion influenced by the r_{offset} . The frequency of the notch shifts similarly to that of the single STO puck calculated from the semi-analytical formula

$$f[\text{GHz}] \approx \frac{34}{a[\text{mm}] \sqrt{\epsilon_r}} \left(\frac{a}{d} + 3.45 \right) \quad (1)$$

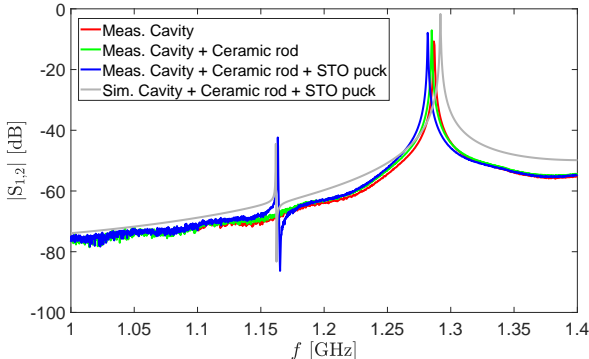
where a and d are the radius and height of the puck, respectively [38]. The frequency sensitivity of modes 1 and 2 is generally lower than that of the notch as shown in Fig. 8(b). Similar to the eigenmode analysis, for ϵ_r below 230, mode 1 is the elliptical cavity-dominant mode, whereas above 230, it becomes the second mode. For the elliptical cavity-dominant mode, frequency sensitivity peaks at $\epsilon_r = 230$, although this is accompanied by a decrease in its phase derivative amplitude that is related to Q -factor value. However, the product of frequency sensitivity and the phase derivative for the two modes is equal to that of the notch for a PEC cavity (Fig. 8(c)),

whereas for a copper cavity (Fig. 8(d)), this product for the notch exceeds that of the two modes. This coupling allows for a trade-off between higher frequency sensitivity and a higher Q -factor, depending on the ϵ_r value.

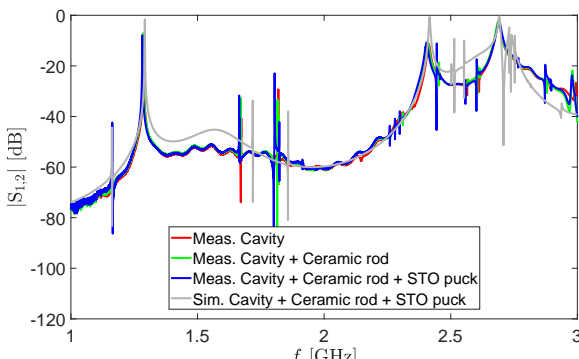
Test measurements. To assess the coupling between the two modes in practice, a test case was established by placing the STO puck inside an elliptical cavity. Excitation is provided through two long rods positioned at the end flanges, and the STO puck is secured at the center of the cavity with a radial offset of 19 mm, mounted on a ceramic rod (see Fig. 9). The resonance of the STO puck, observed at 1.16 GHz in Fig. 9(b), aligns with the predictions from the simulations. This correspondence suggests that the analyses conducted in this section regarding the coupling between the two modes can be considered valid. In addition to the fundamental mode of the STO puck and the elliptical cavity, many other higher-order modes can also be excited in the resonators (as shown in Fig. 9(c)). Depending on the application, one or more of these modes with different frequencies, field patterns, and frequency sensitivities could also be selected for mode coupling.



(a) Measurement setup of the coupled cavity



(b) Measurement results



(c) Measurement results over a wide frequency range

FIG. 9. The measurement setup and results of the coupled elliptical cavity with the STO puck. The STO puck is fixed to the flange via a long ceramic rod at $r_{\text{offset}}=19$ mm. Two long antennas were used for the $S_{2,1}$ measurement: one at the flange center and the other at $r_{\text{offset}}=-19$ mm. Note that the elliptical cavity used for the measurements had a slightly different shape than the one used for the simulations, causing a frequency shift in the resonance modes of the cavity. An ϵ_r of 300 is assumed in the simulation.

IV. DISCUSSION

Coupled dielectric resonators have already been proposed for the realization of sensitive particle and radiation bolometers at frequency around 10 GHz. In the bolometer detector described in Ref. [21–23], two resonators, realized using Sapphire and STO pucks, are positioned one on the top of the other. Their coupling

by fringing fields turns out to be very weak, thus they can be described by using a perturbative theory. Fixed frequency bias of the system then results in a potentially large change in the output amplitude signal at the working frequency. The energy resolution that could be achieved is $\delta E \sim 10^{-23}$ J/Hz at 1 K, 10^{-20} J/Hz at 10 K and 2.5×10^{-19} J/Hz at 30 K. Unlike other high-resolution detectors, the bolometer operates at a relatively high cryogenic temperature in the range between 7 and 30 K. In addition to the detection of single particles, a rapid thermal time constant and a high df/dT response have been demonstrated [21–23].

In our case, the sapphire resonator is replaced with a superconducting cavity and, as a paradigmatic example, we have used an elliptical TESLA-shaped cavity available at CERN. When the STO resonator is positioned inside the cavity, the coupling between the two can be easily controlled by varying the puck's offset and frequency (Sect. III). In particular, the latter can be defined by properly adjusting the physical dimensions of the puck and by taking into account the STO permittivity at the selected working temperature. In this regard, it is important to stress that the results reported in Fig. 5, 7 and 8, which are shown as a function of the STO permittivity and by assuming the geometric parameters of the STO puck described in Sec. II, are valid also for higher values of the STO permittivity such as those found at low temperature.

Given the remarkable change of the STO permittivity as a function of the temperature, we expect that resonators having typical diameter in the range of 1 mm are needed to achieve a significant coupling with the TESLA-shaped cavity at liquid helium temperatures, or below. On the one hand, the heat capacity of the puck, which is directly related to its volume, plays a significant role in the system's effectiveness as a detector. Reducing the puck's size increases sensitivity by amplifying the temperature rise per unit of absorbed energy, thereby enhancing the system's detection capabilities. On the other hand, the coupling may be significantly reduced with a small STO puck. The exploitation of higher microwave modes of the dielectric resonator may constitute an useful resource in this context. Alternative dielectrics have low temperature permittivity values nearer to those considered in the simulations; in particular we have considered rutile resonators, which at 0.8 K show Q -factor of 5.6×10^5 for the mode at 2.6 GHz [40]. However the variation of the permittivity of rutile as a function of temperature is less marked [41], thus coupled resonator systems based on rutile resonators are expected to be less sensitive. Different kinds of superconducting cavities can also be considered to operate at different frequencies.

From the simulations reported in Fig. 5 it results that the two cavities can be tuned either in a strong or weak coupling regime. As expected, at resonance the quality factor of the superconducting cavity progressively decreases as the coupling increases. However, we note that eigenmodes having Q -factor in the $10^5 - 10^6$ range can

still be obtained by adjusting r_{offset} and the detuning of the natural frequencies of superconducting cavity and STO resonator. These values are corroborated by transmission spectra measured at low temperature (Fig. 2), which show that the Q -factor of the STO resonator is in the 10^4 range. This value can potentially be further improved by using opportunely prepared STO pucks. Electromagnetic simulations also show that the frequency and phase shifts of the superconducting cavity are amplified as an effect of the coupling with the STO resonator (Fig. 7). In this regard, the phase derivative of $S_{1,2}$ show a particularly steep response.

We also mention that preliminary tests were carried out to test the stability of the STO mode frequency. In the case of measurements running for hours, the observed drift of the resonance frequency, due to pexternal factors and without any feedback control, was in the range of 50 Hz both for the STO puck measured at 0.1 K and for superconducting cavities measured at 1.7 K. These values are strongly reduced, of about one order of magnitude, for timescales of few seconds or minutes. By improving the experimental set up, and introducing a reference phase-locked loop (PLL) frequency stabilization, it is expected a significant reduction of the frequency drift, thus allowing to exploit phase measurements and further improve the system sensitivity. Additionally, the frequency tuning of the detection cavity can be ensured by the ferroelectricity of the STO and can be obtained by applying a DC electric field to the dielectric resonator. The expected tuning

range is in the order of few percent.

V. CONCLUSIONS

To conclude, we have investigated the coupling between a high- Q superconducting cavity and a STO resonator. This study is critical for ultimately optimizing the STO puck dimensions such that mode coupling occurs at the desired cold temperatures, where the STO's frequency is most responsive to temperature changes. The dielectric constant can reach values higher than 30000 measured at temperature of 0.16 K and frequency of 0.1 GHz with a Q -factor of 10000, and can be very well coupled with a 1.3 GHz TESLA cavity, at least at room temperature. The simulations performed with the given STO dimensions indicate a frequency sensitivity of 2.8 MHz for the notch, corresponding to ε_r around 230, where the coupling is at its maximum. This sensitivity aligns with the pattern predicted by the semi-analytic formula for the STO puck alone. Consequently, this approach allows for precise calculation of the STO puck dimensions, providing the necessary frequency sensitivity for a specific project at the target frequency.

VI. ACKNOWLEDGMENTS

We thank Fritz Casper, Sergio Calatroni, Akira Miyazaki, Walter Venturini, Giovanni Carugno and Marco Affronte for stimulating discussions. A.G. acknowledge financial support from PNRR MUR project ECS_00000033_ECOSISTER and A.C. from PNRR MUR project E63C22002190007 , PE23 , NQSTI.

[1] R. V. Pound and G. A. Rebka, Apparent weight of photons, *Phys. Rev. Lett.* **4**, 337 (1960).

[2] S. Asztalos, G. Carosi, C. Hagmann, D. Kinion, K. van Bibber, M. Hotz, L. J. Rosenberg, G. Rybka, A. Wagner, J. Hoskins, C. Martin, N. Sullivan, D. Tanner, R. Bradley, and J. Clarke, Design and performance of the admx squid-based microwave receiver, *Nuclear Instruments and Methods in Physics Research Section A: Accelerators, Spectrometers, Detectors and Associated Equipment* **656**, 39 (2011).

[3] N. Du, N. Force, R. Khatiwada, E. Lentz, R. Ottens, L. J. Rosenberg, G. Rybka, G. Carosi, N. Woollett, D. Bowring, A. S. Chou, A. Sonnenschein, W. Wester, C. Boutan, N. S. Oblath, R. Bradley, E. J. Daw, A. V. Dixit, J. Clarke, S. R. O'Kelley, N. Crisosto, J. R. Gleason, S. Jois, P. Sikivie, I. Stern, N. S. Sullivan, D. B. Tanner, and G. C. Hilton (ADMX Collaboration), Search for invisible axion dark matter with the axion dark matter experiment, *Phys. Rev. Lett.* **120**, 151301 (2018).

[4] R. H. Parker, C. Yu, W. Zhong, B. Estey, and H. Muller, Measurement of the fine-structure constant as a test of the standard model, *Science* **360**, 191 (2018).

[5] M. Nagel, S. R. Parker, E. V. Kovalchuk, P. L. Stanwick, J. G. Hartnett, E. N. Ivanov, A. Peters, and M. E. Tobar, Direct terrestrial test of lorentz symmetry in electrodynamics to 10^{-18} , *Nature Communications* **6**, 8174 (2015).

[6] A. Lo, P. Haslinger, E. Mizrachi, L. Anderegg, H. Müller, M. Hohensee, M. Goryachev, and M. E. Tobar, Acoustic tests of lorentz symmetry using quartz oscillators, *Phys. Rev. X* **6**, 011018 (2016).

[7] A. Blais, R.-S. Huang, A. Wallraff, S. M. Girvin, and R. J. Schoelkopf, Cavity quantum electrodynamics for superconducting electrical circuits: An architecture for quantum computation, *Phys. Rev. A* **69**, 062320 (2004).

[8] M. Reagor, W. Pfaff, C. Axline, R. W. Heeres, N. Ofek, K. Sliwa, E. Holland, C. Wang, J. Blumoff, K. Chou, M. J. Hatridge, L. Frunzio, M. H. Devoret, L. Jiang, and R. J. Schoelkopf, Quantum memory with millisecond coherence in circuit qed, *Phys. Rev. B* **94**, 014506 (2016).

[9] S. Barzanjeh, M. Wulf, M. Peruzzo, M. Kalaei, P. B. Dieterle, O. Painter, and J. M. Fink, Mechanical on-chip microwave circulator, *Nature Communications* **8**, 953 (2017).

[10] B. J. Bloom, T. L. Nicholson, J. R. Williams, S. L. Campbell, M. Bishof, X. Zhang, W. Zhang, S. L. Bromley, and J. Ye, An optical lattice clock with accuracy and stability at the 10^{-18} level, *Nature* **506**, 71 (2014).

- [11] D. G. Matei, T. Legero, S. Häfner, C. Grebing, R. Weyrich, W. Zhang, L. Sonderhouse, J. M. Robinson, J. Ye, F. Riehle, and U. Sterr, 1.5 μ m lasers with sub-10 mhz linewidth, *Phys. Rev. Lett.* **118**, 263202 (2017).
- [12] N. R. Newbury, Searching for applications with a fine-tooth comb, *Nature Photonics* **5**, 186 (2011).
- [13] C. J. Axline, L. D. Burkhardt, W. Pfaff, M. Zhang, K. Chou, P. Campagne-Ibarcq, P. Reinhold, L. Frunzio, S. M. Girvin, L. Jiang, M. H. Devoret, and R. J. Schoelkopf, On-demand quantum state transfer and entanglement between remote microwave cavity memories, *Nature Physics* **14**, 705 (2018).
- [14] K. S. Chou, T. Shemina, H. McCarrick, T.-C. Chien, J. D. Teoh, P. Winkel, A. Anderson, J. Chen, J. C. Curtis, S. J. de Graaf, J. W. O. Garmon, B. Gudlewski, W. D. Kalfus, T. Keen, N. Khedkar, C. U. Lei, G. Liu, P. Lu, Y. Lu, A. Maiti, L. Mastalli-Kelly, N. Mehta, S. O. Mundhada, A. Narla, T. Noh, T. Tsunoda, S. H. Xue, J. O. Yuan, L. Frunzio, J. Aumentado, S. Puri, S. M. Girvin, S. H. Moseley, and R. J. Schoelkopf, A superconducting dual-rail cavity qubit with erasure-detected logical measurements, *Nature Physics* **10**.1038/s41567-024-02539-4 (2024).
- [15] A. Majumdar, M. Bajcsy, A. Rundquist, and J. Vučković, Loss-enabled sub-poissonian light generation in a bimodal nanocavity, *Phys. Rev. Lett.* **108**, 183601 (2012).
- [16] C. Wang, Y.-L. Liu, R. Wu, and Y.X. Liu, Phase-modulated photon antibunching in a two-level system coupled to two cavities, *Phys. Rev. A* **96**, 013818 (2017).
- [17] C. Bonizzoni, F. Troiani, A. Ghirri, and M. Affronte, Microwave dual-mode resonators for coherent spin-photon coupling, *Journal of Applied Physics* **124**, 194501 (2018).
- [18] B. Aune, R. Bandelmann, D. Bloess, B. Bonin, A. Bosotti, M. Champion, C. Crawford, G. Deppe, B. Dwersteg, D. A. Edwards, H. T. Edwards, M. Ferrario, M. Fouaidy, P.-D. Gall, A. Gamp, A. Gössel, J. Gruber, D. Hubert, M. Hüning, M. Juillard, T. Junquera, H. Kaiser, G. Kreps, M. Kuchnir, R. Lange, M. Leenen, M. Liepe, L. Lilje, A. Mattheisen, W.-D. Möller, A. Mosnier, H. Padamsee, C. Pagani, M. Pekeler, H.-B. Peters, O. Peters, D. Proch, K. Rehlich, D. Reschke, H. Safa, T. Schilcher, P. Schmüser, J. Sekutowicz, S. Simrock, W. Singer, M. Tigner, D. Trines, K. Twarowski, G. Weichert, J. Weisend, J. Wojtkiewicz, S. Wolff, and K. Zapfe, Superconducting tesla cavities, *Phys. Rev. ST Accel. Beams* **3**, 092001 (2000).
- [19] C. Wang, O. S. Melnychuk, C. Contreras-Martinez, Y. Lu, Y. M. Pischalnikov, O. Pronitchev, B. Giaccone, R. Pilipenko, S. Zorzetti, S. Posen, A. Romanenko, and A. Grassellino, Phase-controlled improvement of photon lifetime in coupled superconducting cavities, *Phys. Rev. Appl.* **21**, 024040 (2024).
- [20] B. T. McAllister, G. Flower, L. E. Tobar, and M. E. Tobar, Tunable supermode dielectric resonators for axion dark-matter haloscopes, *Phys. Rev. Appl.* **9**, 014028 (2018).
- [21] L. Hao, J. Gallop, and J. Macfarlane, Coupled microwave resonators for sensitive bolometric detection, *IEEE Transactions on Instrumentation and Measurement* **54**, 886 (2005).
- [22] L. Hao, T. Quincey, G. Lorusso, J. Keightley, J. Chen, and J. Gallop, Sensitive calorimeter based on coupled dielectric resonators, in *2020 Conference on Precision Electromagnetic Measurements (CPMEM)* (2020) pp. 1–3.
- [23] L. Hao, G. Lorusso, and J. C. Gallop, Coupled resonator calorimeter for particle detection, *IEEE Transactions on Instrumentation and Measurement* **70**, 1 (2021).
- [24] J. Breeze, K.-J. Tan, B. Richards, J. Sathian, M. Oxborrow, and N. M. Alford, Enhanced magnetic purcell effect in room-temperature masers, *Nature Communications* **6**, 6215 (2015).
- [25] P. Brun, A. Caldwell, L. Chevalier, G. Dvali, P. Freire, E. Garutti, S. Heyminck, J. Jochum, S. Knirck, M. Kramer, C. Krieger, T. Lasserre, C. Lee, X. Li, A. Lindner, B. Majorovits, S. Martens, M. Matysek, A. Millar, G. Raffelt, J. Redondo, O. Reimann, A. Ringwald, K. Saikawa, J. Schaffran, A. Schmidt, J. Schütte-Engel, F. Steffen, C. Strandhagen, G. Wieching, and M. Collaboration, A new experimental approach to probe qcd axion dark matter in the mass range above $\$ \$\{ 40 \} \backslash \{ \{ \text{upmu} \} \backslash \text{mathrm}\{ \{ \text{ev} \} \} \$ \$$, *The European Physical Journal C* **79**, 186 (2019).
- [26] E. R. Eisenach, J. F. Barry, M. F. O’Keeffe, J. M. Schloss, M. H. Steinecker, D. R. Englund, and D. A. Braje, Cavity-enhanced microwave readout of a solid-state spin sensor, *Nature Communications* **12**, 1357 (2021).
- [27] H. H. Vallabhanupurapu, J. P. Slack-Smith, V. K. Sewani, C. Adambukulam, A. Morello, J. J. Pla, and A. Laucht, Fast coherent control of a nitrogen-vacancy-center spin ensemble using a ktao_3 dielectric resonator at cryogenic temperatures, *Phys. Rev. Appl.* **16**, 044051 (2021).
- [28] Y.-Y. Pai, A. Tylian-Tyler, P. Irvin, and J. Levy, Physics of sratio_3 -based heterostructures and nanostructures: a review, *Reports on Progress in Physics* **81**, 036503 (2018).
- [29] R. A. Cowley, Lattice dynamics and phase transitions of strontium titanate, *Phys. Rev.* **134**, A981 (1964).
- [30] K. A. Müller and H. Burkard, SrTiO_3 : An intrinsic quantum paraelectric below 4 k, *Phys. Rev. B* **19**, 3593 (1979).
- [31] R. Viana, P. Lunkenheimer, J. Hemberger, R. Böhmer, and A. Loidl, Dielectric spectroscopy in sratio_3 , *Phys. Rev. B* **50**, 601 (1994).
- [32] J. F. Schooley, W. R. Hosler, and M. L. Cohen, Superconductivity in semiconducting sratio_3 , *Phys. Rev. Lett.* **12**, 474 (1964).
- [33] R. G. Geyer, B. Riddle, J. Krupka, and L. A. Boatner, Microwave dielectric properties of single-crystal quantum paraelectrics KTaO_3 and SrTiO_3 at cryogenic temperatures, *Journal of Applied Physics* **97**, 104111 (2005).
- [34] M. A. Hosain, J.-M. Le Floch, J. F. Bourhill, J. Krupka, and M. E. Tobar, Ferroelectric phase transition and crystal asymmetry monitoring of SrTiO_3 using quasi $\text{TEm}_{1,1}$ and quasi $\text{TMm}_{1,1}$ modes, *Journal of Applied Physics* **126**, 104102 (2019).
- [35] Z. C. Zhao, M. Goryachev, J. Krupka, and M. E. Tobar, Precision multi-mode dielectric characterization of a crystalline perovskite enables determination of the temperature-dependent phase transitions, *IEEE Transactions on Ultrasonics, Ferroelectrics, and Frequency Control* **69**, 423 (2022).
- [36] D. Davidovikj, N. Manca, H. S. J. van der Zant, A. D. Caviglia, and G. A. Steele, Quantum paraelectricity probed by superconducting resonators, *Phys. Rev. B* **95**, 214513 (2017).
- [37] V. T. Engl, N. G. Ebensperger, L. Wendel, and M. Scheffler, Planar ghz resonators on sratio_3 : Suppressed losses at temperatures below 1 k (2019), arXiv:1911.11456 [cond-mat.supr-con].

- [38] D. Kajfez and P. Guillon, *Dielectric Resonators*, Artech House microwave library (Noble Publishing Corporation, 1998).
- [39] D. Pozar, *Microwave Engineering* (Wiley, 2012).
- [40] A. Cassinese, to be published.
- [41] R. A. Parker, Static dielectric constant of rutile (tio_2), 1.6-1060°k, Phys. Rev. **124**, 1719 (1961).